

One-dimensional array of ion chains coupled to an optical cavity

This article has been downloaded from IOPscience. Please scroll down to see the full text article.

2013 New J. Phys. 15 053001

(<http://iopscience.iop.org/1367-2630/15/5/053001>)

View [the table of contents for this issue](#), or go to the [journal homepage](#) for more

Download details:

IP Address: 18.51.3.76

The article was downloaded on 20/06/2013 at 19:30

Please note that [terms and conditions apply](#).

One-dimensional array of ion chains coupled to an optical cavity

Marko Cetina¹, Alexei Bylinskii⁴, Leon Karpa, Dorian Gangloff, Kristin M Beck, Yufei Ge, Matthias Scholz², Andrew T Grier³, Isaac Chuang and Vladan Vuletić

Department of Physics, MIT-Harvard Center for Ultracold Atoms, and Research Laboratory of Electronics, Massachusetts Institute of Technology, Cambridge, MA 02139, USA

E-mail: abyl@mit.edu

New Journal of Physics **15** (2013) 053001 (14pp)

Received 6 February 2013

Published 1 May 2013

Online at <http://www.njp.org/>

doi:10.1088/1367-2630/15/5/053001

Abstract. We present a novel system where an optical cavity is integrated with a microfabricated planar-electrode ion trap. The trap electrodes produce a tunable periodic potential allowing the trapping of up to 50 separate ion chains aligned with the cavity and spaced by $160\ \mu\text{m}$ in a one-dimensional array along the cavity axis. Each chain can contain up to 20 individually addressable Yb^+ ions coupled to the cavity mode. We demonstrate deterministic distribution of ions between the sites of the electrostatic periodic potential and control of the ion–cavity coupling. The measured strength of this coupling should allow access to the strong collective coupling regime with $\lesssim 10$ ions. The optical cavity could serve as a quantum information bus between ions or be used to generate a strong wavelength-scale periodic optical potential.

¹ Currently at IQOQI, Innsbruck, Austria.

² Currently at TOPTICA Photonics AG, R&D Division, Lochhamer Schlag 19, D-82166 Gräfelfing, Germany.

³ Currently at École Normale Supérieure, Paris, France.

⁴ Author to whom any correspondence should be addressed.



Content from this work may be used under the terms of the [Creative Commons Attribution 3.0 licence](https://creativecommons.org/licenses/by/3.0/). Any further distribution of this work must maintain attribution to the author(s) and the title of the work, journal citation and DOI.

Contents

| | |
|--|-----------|
| 1. Introduction | 2 |
| 2. Experimental set-up and trap fabrication | 4 |
| 3. Deterministic splitting of ion crystals | 7 |
| 4. Ion–cavity coupling | 8 |
| 5. Motional spectroscopy | 11 |
| 6. Conclusion | 12 |
| Acknowledgments | 12 |
| References | 12 |

1. Introduction

The coupling of trapped atomic ions to optical cavities constitutes a promising route for scaling quantum information processing (QIP) to larger ion numbers and exploring a range of possibilities in quantum simulation (QSim). Ions are an ideal building block for both QIP [1, 2] and QSim [3–5] thanks to exquisite individual control and strong, long-range Coulomb interactions. These properties have enabled quantum gate fidelities close to the threshold where error correction protocols could guarantee fault-tolerant computation [6]. Entanglement of up to 14 ions has been achieved [7], small spin networks of up to nine spins have been simulated [8–11], and tunable interactions have been successfully engineered in networks with hundreds of spins [12, 13]. All the schemes that have achieved these milestones involve coupling the internal states of ions via the collective motional modes of Coulomb crystals that are formed when ions are trapped in the same trap. Unfortunately, the increasing number of these collective motional modes in bigger ion crystals makes it difficult to scale this approach to larger ion numbers. One way around these limitations is to interface ions with a quantum bus in the form of ‘transport’ ions, photons or phonons.

One possible realization of a quantum bus is to physically transport ions [14, 15]; this requires reconfigurable multi-zone traps and the ability to deterministically split ion crystals and move ions without decoherence of the internal states that are used for storing the quantum information [16]. Quantum teleportation has been achieved in such a system [17], and the full toolbox for QIP has been demonstrated [18], including transport with very little motional heating [19].

A photon-based quantum bus between ions is attractive because optical qubits are robust against decoherence over long distances. Free-space coupling between photons and ions is weak, but has potential in probabilistic schemes [20, 21]. Two ions have been entangled via a long-distance photon bus in a probabilistic scheme with 10^{-8} success probability [22, 23]. Scalable, deterministic photon-based schemes require an efficient, coherent ion–photon interface that can be provided by an optical cavity. High cavity finesse and small optical mode area are two ways to reach strong coupling between cavity photons and atoms or ions [24–27]. Another approach is to couple cavity photons to an ensemble of many atoms or ions so as to reach the strong collective coupling regime [28, 29].

Coupling of a single ion to a cavity has been demonstrated on a strong dipole transition [30, 31] and on a weak quadrupole transition with the drawback of slow coupling, susceptible to

technical decoherence [32]. A high-finesse cavity coupled to the weak leg of the Raman S–P–D transition in a Ca^+ ion has enabled motional-sideband-resolved Raman spectroscopy [33, 34] and efficient single photon generation [34–36]. This has led to fast, high-fidelity and tunable entanglement between an ion and the polarization state of the output photon [37]. Despite these advances, fast coherent coupling between single ions and cavities remains a challenge. Short micro-cavities, which enable the strong coupling regime for neutral atoms [26, 27] are promising, but have so far been difficult to combine with ion traps because of light-induced charging of the dielectric mirrors resulting in strong time-varying forces on the ions [38].

Strong collective coupling between a cavity and separate ensembles of neutral atoms in the cavity has been used to entangle these ensembles via the cavity mode [39]. However, the use of a cavity photon bus for entanglement of separate ion ensembles has not yet been demonstrated. One natural benefit of doing this with ions is the strong Lamb–Dicke confinement by the electric fields which reduces decoherence of the collective states sensitive to spatial phase [40–42]. A more important benefit is the ability to combine the cavity photon bus with the QIP tools utilizing the common motional modes of co-trapped ions [43]. Strong collective coupling between a large three-dimensional (3D) Coulomb crystal of ions and a cavity has been achieved [29], leading to the observation of cavity electromagnetically induced transparency [44]. Single-ion addressability, motional mode control and ground-state cooling are all difficult to achieve in 3D Coulomb crystals, one of the challenges being strong trap-driven radio-frequency micromotion. These problems can be avoided in one-dimensional (1D) ion chains, which would therefore yield a more promising system when coupled to an optical cavity.

Another possibility for realizing a quantum bus between ions is through the exchange of phonons between microtraps [45–47]. Since this type of coupling scales as d^{-3} , where d is the separation between microtraps, the individual microtraps need to be closely spaced. Sufficiently small-scale traps are difficult to operate in view of thermally activated heating of ions in close proximity to trap electrodes that scales roughly as r^{-4} , where r is the distance of ions to the electrodes and is of order d [1]. Nonetheless, coherent exchange of phonons in pairs of microtraps separated by a few tens of μm has been demonstrated with single-phonon Rabi frequencies of a few kHz [48, 49]. The coupling can be enhanced by introducing more ions in each microtrap, and the scaling with ion number has been experimentally shown to be faster than linear [49].

An alternative way to realize small-scale microtraps is to trap ions in an optical lattice, where the length scale is that of an optical wavelength. Although optical trapping of ions is difficult, single ions have been trapped in an optical dipole trap for milliseconds [50], and in optical lattices for microseconds [51, 52] with a more recent demonstration of 10 ms trapping times [53]. A major challenge here is for the optical dipole force from the lattice to overcome the large electric forces acting on the charge of the ion. An optical cavity is a convenient way to build up very high lattice intensities for this purpose.

Ions in optical lattices are also promising for QSim in periodic potentials. Compared to neutral atoms interacting via short-range, next-neighbor interactions [54, 55], ions in optical lattices would enable the study of systems with strong long-range interactions. In one dimension, the interplay between Coulomb interactions in an ion crystal and an incommensurate periodic potential can lead to phase transitions that are of interest in both the classical and quantum regimes in the context of the Frenkel–Kontorova model [56–58]. This model is closely related to energy transport in crystals and friction, and is of considerable interest in several

domains of physics. Optical lattices can be extended to two and three dimensions, where frustrated spin Hamiltonians [47] and synthetic gauge fields [59] could be simulated with ions. Imaging individual particles in lattice sites is a capability of great interest for QSim in periodic potentials, and recently single-site resolution has been reached for neutral atoms [60, 61]. Ions in optical lattices naturally separate by many lattice sites owing to their strong Coulomb repulsion. The resulting large separations and the ability to freeze ions in space using tight electrostatic potentials are promising for high-resolution imaging of ion positions in a lattice. Such imaging would be conducive to studying many of the mentioned models.

We present a novel system where all three possibilities for a quantum bus (ionic, photonic and phononic) as well as the behavior of ions in periodic potentials can be explored. This is enabled by tunable periodic electrostatic and optical potentials and strong collective coupling of ions to an optical cavity. To our knowledge, this is the first system to integrate an optical cavity with a microfabricated planar-electrode ion trap, producing a very versatile platform for QIP and QSim with ions and photons.

Our microfabricated planar-electrode ion trap features a linear Paul trap with a novel design of the inner electrode, which allows the Paul trap to be split into a periodic array of 50 separate traps by a tunable electrostatic potential. The sites of the array are separated by $160\ \mu\text{m}$ and can each hold up to 20 individually-addressable Yb^+ ions, stretched out in chains (1D Coulomb crystals) along the null line of the two-dimensional (2D) quadrupole RF driving field and along the mode of an optical cavity (see figure 1). By increasing axial confinement, these chains can be transformed into higher-dimensional crystal structures [62–64]. In addition, 24 DC electrodes on the microfabricated trap allow the shaping of quartic potentials along the cavity, local control of secular frequencies at different sites of the array, as well as accurate micromotion compensation along the length of the array, which we measure spectroscopically using the optical cavity. We achieve deterministic control of ion distribution between the sites of the array, and control of ion–cavity coupling. Our measurements of fluorescence into the cavity indicate an achievable strong collective coupling with around ten ions in a single array site. The demonstrated controls of micromotion, of distribution of ions between array sites, and of the cavity coupling are important for achieving high fidelity of interaction of the ion chains with the cavity photon bus [43], as well as high fidelity of ion [16] or phonon exchange [46] between the chains, the latter benefiting from enhanced Coulomb coupling due to a large number of ions per chain [49].

The optical cavity in our system can also be used to generate an intra-cavity standing wave with a maximum intensity of $20\ \text{W mm}^{-2}$, resulting in a deep all-optical periodic potential for the ions with a periodicity of $185\ \text{nm}$, which is three orders of magnitude smaller than the periodicity of the trap array. This makes our system attractive for QIP with ions in optical microtraps [45, 46] and for QSim with ions in periodic potentials [56–58]. In particular, together with the rich electrode structure, the optical potential provides us with local control of phonon couplings, which can be engineered to study various interesting Hamiltonians, including spin frustration [47] and synthetic gauge fields [59] in 2D ion crystal phases that can be produced in the array sites by strong axial confinement, although driven micromotion cannot be compensated in this case and must be taken into account.

2. Experimental set-up and trap fabrication

The centerpiece of the experimental set-up is a planar-electrode linear Paul trap placed between the mirrors of a $22\ \text{mm}$ -long optical cavity. The maximum finesse of the cavity is 1.25×10^4 and

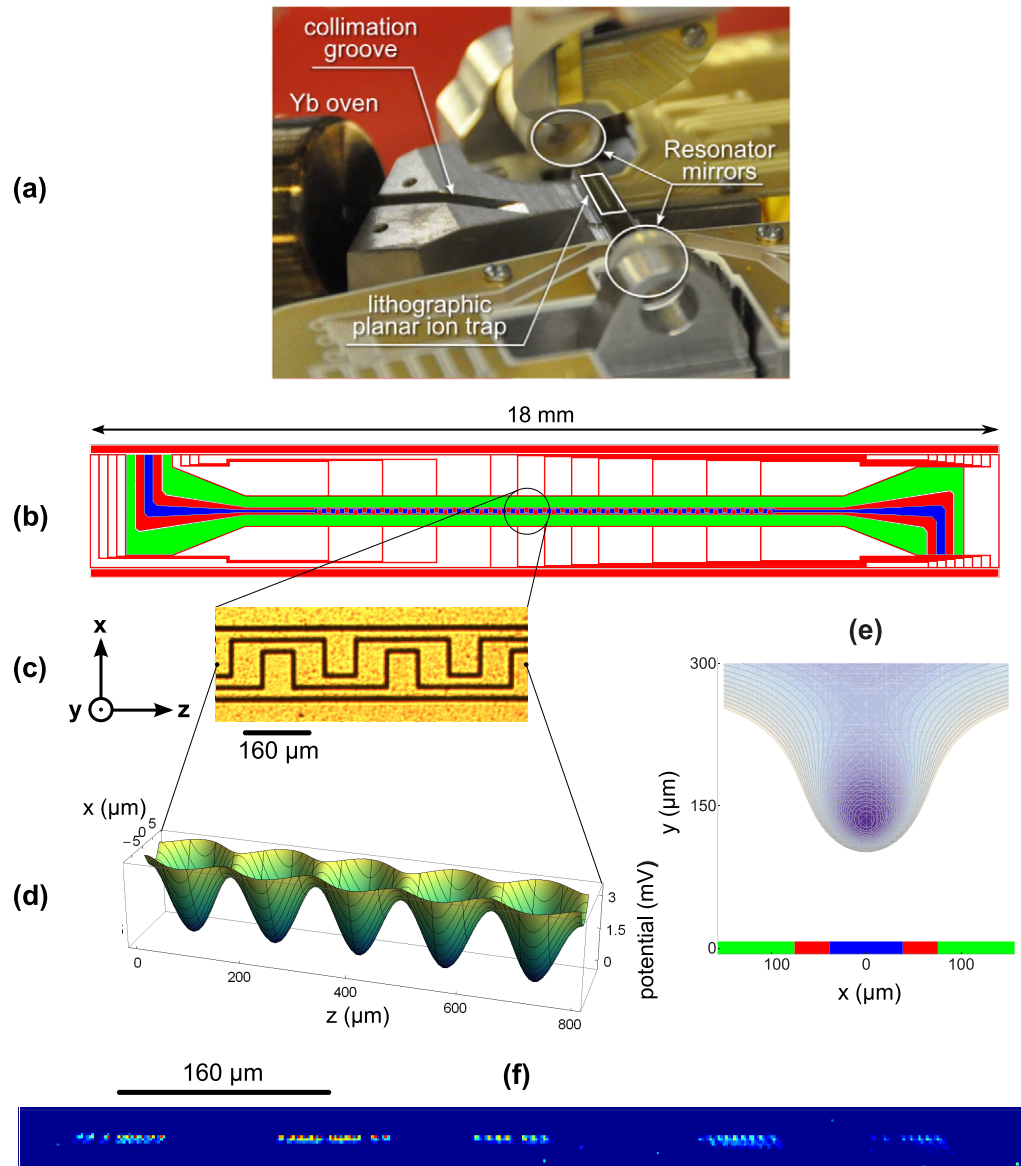


Figure 1. (a) A picture of the experimental set-up, with the microfabricated planar-electrode ion trap, the 22 mm-long optical cavity, and the Yb oven. (b) Layout of the microfabricated trap chip. Outer RF electrodes are shown in green, and the inner RF electrode is split into three periodic electrodes shown in blue and red. The 24 large rectangular DC electrodes are shown in white. (c) A portion of the inner periodic electrodes generating the electrostatic periodic potential. (d) Periodic potential at the position of the ions $138 \mu\text{m}$ above the trap surface for a -1 V DC voltage applied to the inner periodic electrode (blue) and $+0.9 \text{ V}$ to the outer periodic electrodes (red). (e) Pseudopotential produced in the radial directions by the RF voltage applied to the outer RF electrodes. The equipotential contours are spaced by 5 mV . (f) Image of five array sites containing small ion chains where single ions can be resolved. The ions are illuminated by light in the cavity mode, which is overlapped with the array.

the TEM₀₀ mode waist is 38 μm , corresponding to a calculated antinode cooperativity $\eta = 0.23$ (η is defined in section 4, equation (1)) for the 369 nm $^2\text{S}_{1/2} - ^2\text{P}_{1/2}$ transition in the Yb⁺ ion. The trapping region of the Paul trap consists of the central 8 mm of the RF quadrupole nodal line, which is overlapped with the mode of the cavity by careful alignment [65]. A split central electrode with a periodic structure, shown in figure 1(c), allows the long trap to be sectioned into 50 separate trapping sites along the cavity mode, spaced by 160 μm , by applying a negative DC voltage to the inner periodic electrode and a positive DC voltage to the outer periodic electrodes. The ratio of outer-electrode voltage to inner-electrode voltage of -0.9 was chosen to cancel the displacement of the trap in the direction perpendicular to the chip surface. Confinement in the plane perpendicular to the cavity axis is achieved by applying an RF voltage of 127 V amplitude at $\omega_{\text{RF}} = 2\pi \times 16.4$ MHz to the two long outer electrodes shown in green in figure 1(d) and grounding the rest of the trap at RF frequencies. The resulting Paul trap resides 134 μm from the electrode surface, has trap frequencies $\omega_{x,y} = 2\pi \times 1.3$ MHz, a Mathieu parameter $q = 0.22$ and a trap depth of 84 meV along the weakest confinement direction away from the chip surface (pseudopotential shown in figure 1(e)). In practice, the trap depth is usually increased to a few hundred meV by applying a DC quadrupolar field that provides additional confinement along the weak axis at the expense of deconfinement along the other axis. This is achieved by applying a negative DC voltage of a few volts to the RF electrodes. As a result of this DC quadrupole field, the x - and y -trap frequencies differ by a few hundred kHz. The trap is equipped with 24 DC electrodes for finely shaping the potential along the linear dimension of the trap, and for compensating stray electric fields in the RF trapping (transverse) plane (figure 1(b)).

The trap was fabricated on a 500 μm -thick single-crystal quartz wafer using a procedure similar to the one described in [66]. The wafer was mechanically cleaned using Clorox 409 surfactant, followed by a 30 min soak in a 3 : 1 solution of H₂SO₄ : H₂O₂ at room temperature and a 20 min soak in 4 : 1 : 1 H₂O : NH₄OH : H₂O₂ at 65 °C. A 10 nm Ti adhesion layer was evaporated using an electron beam, followed by a 300 nm-thick Ag layer. The trap pattern was defined using 6 μm -thick AZ4620 positive photoresist exposed through a soft contact chrome mask. The trapping electrodes were produced by electroplating a 1.7 μm -thick layer of Au onto the exposed Ag with 8 $\mu\text{A mm}^{-2}$ current density (single-polarity) using Transene TSG-250 sulfite Au-plating solution in a stirred 49 °C bath. To electrically separate the trapping electrodes, the AZ4630 photoresist was removed by acetone, followed by a 20 s Ag etch in 1 : 1 : 4 H₂O₂ : NH₄OH : H₂O and a 5 s Ti etch in 1 : 4 HF : H₂O. The wafer was then protected with 1–2 μm -thick NR9-3000P photoresist and cut into individual 2.3 mm \times 18 mm traps on a carbide die saw. Given that our material processing steps were identical to the ones used in [66], we expect the heating rate of ions trapped 134 μm from the trap surface to be on the order of $h \times 1$ MHz ms⁻¹, where h is Planck's constant.

The cavity mirrors were coated by Advanced Thin Films (Boulder, CO) with a dielectric stack structure of SiO₂ and Ta₂O₅ (top layer) with a 2 : 1 thickness ratio. Mirror transmission was quoted as $T = 1.8 \times 10^{-4}$ at 369 nm. Before the set-up was inserted into the vacuum chamber, the finesse was measured to be $F_0 = 1.25 \times 10^4$. Under vacuum, the finesse has been degrading steadily over time, with mirror loss (L) increasing linearly at a rate of 6×10^{-5} per month ($F = \pi/(T + L)$). The experimental results presented are for a finesse of $F_1 = 2400$. The finesse may be restored by oxygen treatment [67] before implementing efficient quantum information protocols with ions, but certain proof-of-principle experiments can be performed with the current set-up.

Yb⁺ ions are produced by a two-step photo-ionization [68, 69] of the effusive atom flux from a resistively heated oven. The flux is collimated, and to avoid coating the trap, angled away

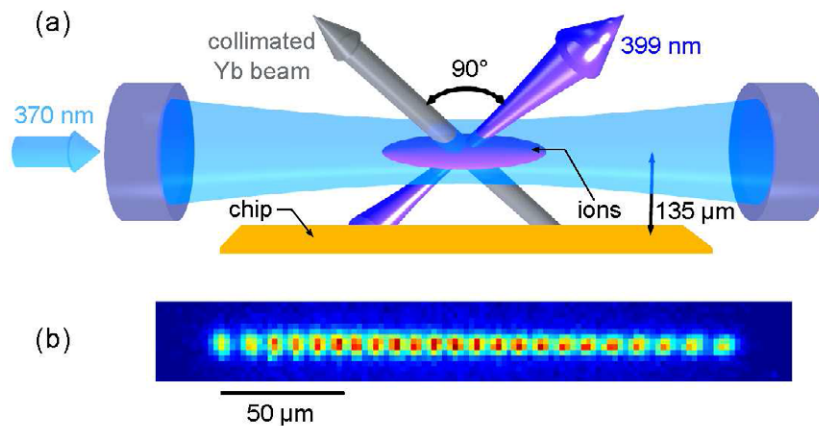


Figure 2. (a) Trap loading configuration. 399 nm light perpendicular to the thermal atom beam excites the isotope of choice to the 1P_1 state, from which ionization to the continuum proceeds via the cavity-enhanced 369 nm light. (b) Isotopically pure 1D crystal of 23 ions of $^{174}\text{Yb}^+$ in a harmonic potential. Ions of a different isotope would be off-resonant with the excitation light and would appear as dark gaps in the chain.

from the chip surface (see figure 1(a)). The ionization is accomplished by resonant excitation on the 399 nm $^1S_0 - ^1P_1$ neutral Yb transition perpendicular to the oven flux, combined with one-photon ionization via 369 nm light built up in the resonator mode (see figure 2(a)). The intra-cavity intensity of the 369 nm light can be continuously controlled up to a maximum of 20 W mm^{-2} , resulting in a typical loading rate of $\sim 2 \text{ ions s}^{-1}$. Addressing the coldest direction (perpendicular to the flux) of the atomic beam with the 399 nm light minimizes Doppler broadening and resolves the different Yb isotopes of interest, which are spaced by at least $2\pi \times 250 \text{ MHz}$ in frequency. This allows us to achieve isotopic purity of our ion samples in excess of 90% (see figure 2(b)). In principle, the remaining undesired isotopes can be pushed to one side by radiation pressure prior to crystallization, and after crystallization into a chain, they can be separated using the crystal splitting method discussed in the next section.

3. Deterministic splitting of ion crystals

Our ability to control the loading rate and the shape of the axial potential permits the loading of a controlled number of ions into a long isotopically pure 1D crystal in the trapping region. By applying a DC periodic potential, we can split this crystal into smaller 1D crystals at the individual array sites with up to 20 ions per site. Crystals longer than 20 ions per site merge across sites, given the radial confinement achievable in our system and the corresponding maximum axial confinement before the onset of structural phase transitions from 1D to 2D and 3D crystals [62–64], although these higher-dimensional phases with more ions might be an interesting platform for studying quantum magnetism [47]. The crystal order of our sample resulting from the strong ion–ion repulsion pins each ion with respect to the applied periodic potential, causing the ion crystal to be split at defined positions and resulting in a deterministic loading of the trap array. By ramping the periodic potential up and down multiple times and

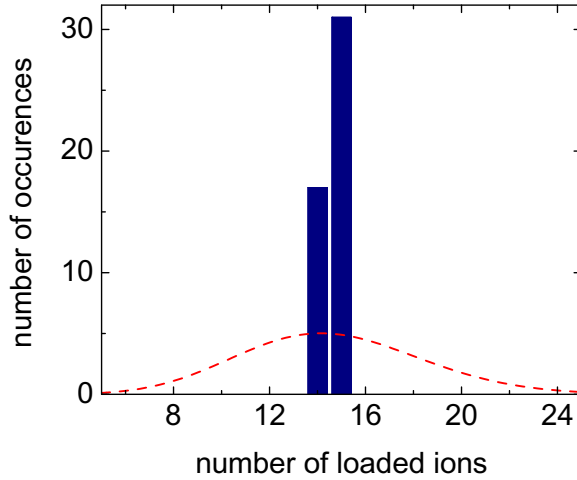


Figure 3. Typical ion number histogram for an array site after splitting a longer chain repeatedly with the periodic potential. The red dotted curve is the Poisson distribution with identical mean. The Fano factor at this site is 1.6%. The Fano factor at any site of the array is $< 10\%$, limited by residual isotopic impurity.

counting the number of ions loaded into each array site, we collect statistics that show highly suppressed ion number fluctuations, as shown in figure 3. This can be quantified using the Fano factor, which is defined as the ratio of the ion number variance to the mean number of ions loaded in each trap. This factor is unity for a Poisson process, which would be expected for weak interactions. We typically observe Fano factors less than 0.1. In addition, by shaping the overall axial potential appropriately, we can control the mean number of ions loaded into each trap.

4. Ion–cavity coupling

In free space, the probability of dipole interaction between a photon and a two-level ion can be quantified by the absorption probability, given by the ratio of the resonant atomic photon scattering cross-section $\frac{3}{2\pi}\lambda_0^2$ to the mode area $\frac{1}{2}\pi w^2$ of a Gaussian laser beam, where $\lambda_0 = 2\pi/k_0$ is the resonant wavelength and w is the mode waist [24]. In free space, this ratio is substantially smaller than unity as diffraction limits the waist size. One solution is an optical cavity, which enhances the interaction probability by the number of round trips F/π in the cavity (where F is the cavity finesse) and a factor of 4 at the antinode of the standing wave. The result is the single particle antinode cooperativity [24]

$$\eta = \frac{24F}{\pi w^2 k_0^2} = \frac{4g^2}{\kappa\Gamma}, \quad (1)$$

which is the figure of merit in cavity quantum electrodynamics, encapsulating the strength of atom–cavity coupling g (single photon Rabi frequency $2g$) relative to the cavity decay rate constant κ and the atomic spontaneous emission rate constant Γ . (Note that the second expression can be generalized to any transition in a multi-level ion by using the appropriate g and Γ , while the first expression is only applicable to a two-level system.) A coherent ion–photon interface necessitates the strong coupling regime $\eta \gtrsim 1$, which can be achieved

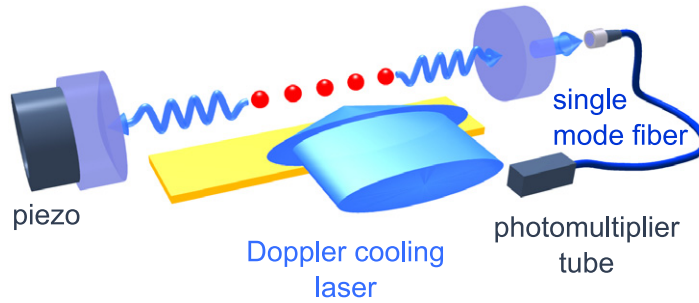


Figure 4. Set-up for fluorescence spectroscopy via the cavity. Doppler cooling light perpendicular to the cavity-trap axes is scattered into the cavity, which acts as a tunable spectrometer. The light exiting the cavity is coupled to a single-mode fiber and detected by a PMT. For results presented here, incident light is linearly polarized in the direction perpendicular to the cavity-trap axes, and collected photons are polarization-analyzed in the same direction.

with a high finesse F (by increasing the mirror reflectivity), or by using micro-cavities with a small waist w . Alternatively, by coupling a cavity to an ensemble of N ions, the collective cooperativity is enhanced by the factor N and the strong collective coupling regime is achieved for $N\eta \gtrsim 1$.

In order to quantify the coupling between the trapped ions and the cavity mode in our system, we use the set-up shown in figure 4. $^{174}\text{Yb}^+$ ions held in the planar trap are Doppler-cooled on the $^2\text{S}_{1/2}$ – $^2\text{P}_{1/2}$ transition ($^2\text{P}_{1/2}$ state natural linewidth $\Gamma = 2\pi \times 19.6$ MHz [70]) using a linearly-polarized laser beam perpendicular to the cavity-trap axis with polarization also perpendicular to the cavity-trap axis. The intensity of the cooling light is $I = 15$ mW mm $^{-2}$, corresponding to the resonant saturation parameter $s_0 = \frac{1}{3}I/I_{\text{sat}} = 10$ of the Π transition, where $I_{\text{sat}} = 0.508$ mW mm $^{-2}$ is the saturation intensity. The ion fluorescence photons scattered into the cavity mode are polarization-analyzed, coupled into a single-mode fiber and counted using a photomultiplier tube (PMT). When the cavity is resonant with the cooling light and detuned from the atomic resonance by $\delta = 2.5\Gamma$, and when only photons with the same linear polarization as the incident light are collected, we observe 350 count s $^{-1}$ from a single ion in a weak axial potential (peak value in figure 5). The ion in this case is not localized with respect to the cavity standing wave. The collected photon flux is consistent with the expected cooperativity of $\eta = 0.044$ for a finesse of $F_1 = 2400$, as explained below.

The total scattering rate into free space for the given saturation and detuning is $\Gamma_{\text{sc}} = \frac{s}{1+s} \frac{\Gamma}{2} = 1.7 \times 10^7$ s $^{-1}$, of which a fraction $1/(1+s) = 0.72$ is coherent, where $s = s_0/(1 + (\frac{2\delta}{\Gamma})^2)$ is the saturation parameter [71]. Of these, a fraction $\frac{1}{2}\eta\kappa/(\kappa + \Delta\omega_{\text{laser}})$ is collected by the cavity, where the antinode cooperativity η is multiplied by 1/2 for averaging over the cavity standing wave, and by the spectral overlap of the cavity and the laser. The cavity linewidth is $\kappa = 2\pi \times 2.7$ MHz and the laser linewidth $\Delta\omega_{\text{laser}} = 2\pi \times 4.9$ MHz. The incoherently scattered photons are broader in frequency than the cavity linewidth and are not collected efficiently. Of all the photons that do make it into the cavity, only $T/(T+L) = 13\%$ are coupled out due to losses at the mirrors. Since the cavity is symmetric and we observe only one port, 1/2 of the photons are lost through the other port. In addition, we project collected photons onto the same linear polarization as the excitation beam, resulting in a squared Clebsch–Gordan coefficient of 1/3 for

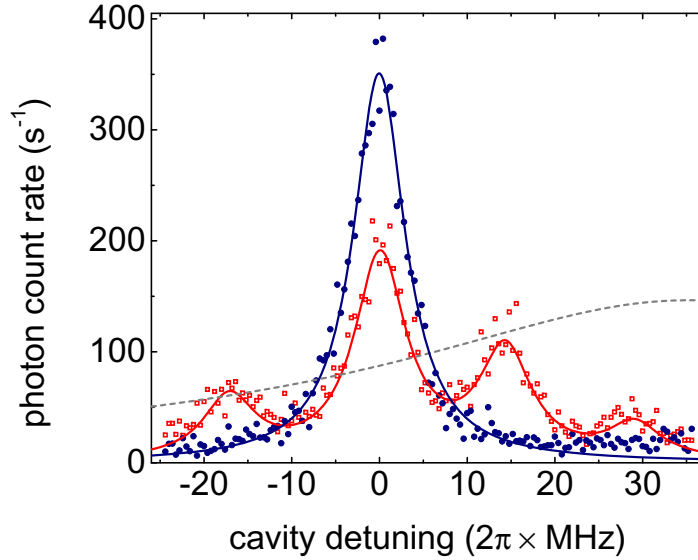


Figure 5. Single-ion fluorescence spectra collected by the cavity for a well-compensated ion (blue) and an ion decompensated (red) in the direction of the Doppler cooling beam by a DC electric field of 65 V m^{-1} . The first-order micromotion sidebands show up clearly and a second-order sideband is also visible on one side. The asymmetry in the spectrum is due to higher scattering rate on the side closer to atomic resonance; the gray dotted curve shows the calculated dependence of the photon scattering rate on the detuning.

the Π transition $J = \frac{1}{2} \rightarrow J = \frac{1}{2}$. Finally, after including cavity-to-fiber mode matching of 0.9, transmission through all the optics of 0.7 and a PMT quantum efficiency of 0.28, the expected count rate of $\sim 370 \text{ count s}^{-1}$ matches the observed count rate of $\sim 350 \text{ count s}^{-1}$ within 10%.

For purely coherent processes within the cavity, such as the transfer of quantum information between ion chains via the cavity mode, of the stated factors degrading our photon collection efficiency, only the squared Clebsch–Gordan coefficient and the cavity standing wave averaging are relevant. By localizing the ion with respect to the cavity standing wave, the full antinode cooperativity η may be recovered, modulo the squared Clebsch–Gordan coefficient. An additional advantage of localizing the ions to better than the mode wavelength (Lamb–Dicke regime) is to reduce motional decoherence. This approach has been used to extend light storage times in atomic ensembles from microseconds [40] to a hundred milliseconds by localizing them in optical lattices with the added challenge of careful AC Stark shift compensation [41, 42]. The longest light storage time of 240 ms was achieved in a Mott insulator, limited by tunneling and lattice heating [72], which, together with AC Stark shifts, are absent or negligible in a Paul ion trap.

We demonstrate precise positioning with respect to the cavity standing wave by confining the ion in the strong axial potential of the periodic array with an axial vibration frequency of $\omega_{\text{ax}} = 2\pi \times 1.14 \text{ MHz}$, and moving it along the cavity axis. We observe a periodic variation of fluorescence scattered into the cavity (shown in figure 6), which corresponds to the spatial modulation of ion–cavity coupling between the node and antinode of the cavity mode (a similar technique was used in [30]). For the ion in figure 6, the fringe visibility is 65%, corresponding

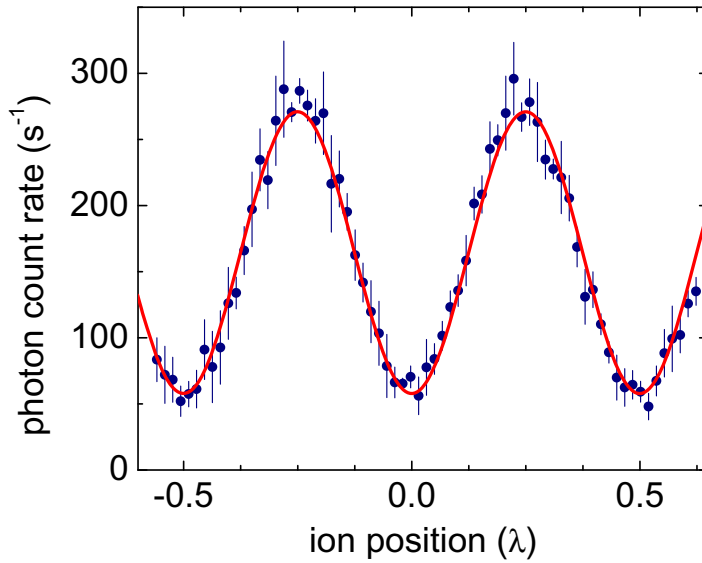


Figure 6. Single-ion fluorescence collected by the cavity resonant with the excitation laser as a localized ion is transported along the cavity mode. The observed mode visibility is 65%, corresponding to an ion temperature of $1.6T_{\text{Doppler}}$ and a thermal rms spread of the ionic wavepacket of 27 nm.

to a temperature of $1.6T_{\text{Doppler}}$ (where $T_{\text{Doppler}} = \frac{1}{2}\hbar\Gamma/k_{\text{B}}$ is the Doppler limited temperature), an ion localized to 27 nm (wavefunction rms spread), and a recovery of antinode η to 80%. These numbers could be further improved using sideband cooling techniques.

With the observed value $\eta = 0.044$, corresponding to a cavity finesse of $F_1 = 2400$, the effective cooperativity parameter approaches unity for an ensemble of about 20 ions. At the initial, undegraded cavity finesse of $F_0 = 1.25 \times 10^4$, this is reduced to about 5 ions per array site.

5. Motional spectroscopy

The spectrum of light scattered into the cavity mode by the ions can be measured by scanning the cavity length at a fixed ion excitation laser frequency (see figure 4). The resolution is limited only by the convolved linewidths of the drive laser $\Delta\omega_{\text{laser}}$ and of the cavity κ , which combine to give $\Delta\omega_{\text{res}} = 2\pi \times 7.5$ MHz. This is sufficiently narrow to resolve the micromotion sidebands resulting from the RF trap drive at $2\pi \times 16$ MHz and to accurately minimize them by compensating the position of the ion relative to the RF null using the DC electrodes (figure 5). This step is important in minimizing motional heating of ions. In addition, it allows us to verify that there is no parasitic micromotion along the cavity axis, which would degrade the fidelity of interaction between ions and cavity photons by spreading the ion spectrum into the micromotion sidebands. This method of micromotion compensation is an alternative to more standard techniques [73] and gives a direct measure of the sideband strength relative to the carrier. (Note that a similar method was used in [34].)

6. Conclusion

We have built and characterized a novel quantum system where ion-based QIP can be interfaced with a phonon bus between microtraps or a cavity-based photon bus, and where light forces could be used to construct 1D Hamiltonians of particles with strong long-range interactions in a periodic potential. This system presents a rich Hilbert space spanned by the internal atomic, phononic and photonic degrees of freedom, where competing interactions could be studied in addition to digital quantum computation.

Acknowledgments

We acknowledge resources provided by the research group of Karl Berggren in the ion trap fabrication process. This work was supported by the Army Research Office (ARO) and the National Science Foundation (NSF). AB and DG gratefully acknowledge support by the National Science and Engineering Research Council of Canada (NSERC) and LK gratefully acknowledges support by the Alexander von Humboldt Foundation. KB gratefully acknowledges support from the National Science Foundation (NSF) through the Graduate Research Fellowship (0645960) and Interdisciplinary Quantum Information Science and Engineering (0801525) programs.

References

- [1] Blatt R and Wineland D 2008 *Nature* **453** 1008–15
- [2] Häffner H, Roos C and Blatt R 2008 *Phys. Rep.* **469** 155–203
- [3] Johanning M, Varón A F and Wunderlich C 2009 *J. Phys. B: Atom. Mol. Opt. Phys.* **42** 154009
- [4] Blatt R and Roos C F 2012 *Nature Phys.* **8** 277–84
- [5] Schneider C, Porras D and Schaetz T 2012 *Rep. Prog. Phys.* **75** 024401
- [6] Benhelm J, Kirchmair G, Roos C F and Blatt R 2008 *Nature Phys.* **4** 463–6
- [7] Monz T, Schindler P, Barreiro J, Chwalla M, Nigg D, Coish W, Harlander M, Hänsel W, Hennrich M and Blatt R 2011 *Phys. Rev. Lett.* **106** 130506
- [8] Friedenauer A, Schmitz H, Glueckert J T, Porras D and Schaetz T 2008 *Nature Phys.* **4** 757–61
- [9] Kim K, Chang M S, Korenblit S, Islam R, Edwards E E, Freericks J K, Lin G D, Duan L M and Monroe C 2010 *Nature* **465** 590–3
- [10] Islam R *et al* 2011 *Nature Commun.* **2** 377
- [11] Kim K *et al* 2011 *New J. Phys.* **13** 105003
- [12] Britton J W, Sawyer B C, Keith A C, Wang C C J, Freericks J K, Uys H, Biercuk M J and Bollinger J J 2012 *Nature* **484** 489–92
- [13] Biercuk M J, Uys H, Vandevender A P, Shiga N, Itano W M and Bollinger J J 2009 *Quantum Inform. Comput.* **9** 920–49
- [14] Hensinger W K, Olmschenk S, Stick D, Hucul D, Yeo M, Acton M, Deslauriers L, Monroe C and Rabchuk J 2006 *Appl. Phys. Lett.* **88** 034101
- [15] Crick D R, Donnellan S, Ananthamurthy S, Thompson R C and Segal D M 2010 *Rev. Sci. Instrum.* **81** 013111
- [16] Kielpinski D, Monroe C and Wineland D J 2002 *Nature* **417** 709–11
- [17] Barrett M D *et al* 2004 *Nature* **429** 737–9
- [18] Home J P, Hanneke D, Jost J D, Amini J M, Leibfried D and Wineland D J 2009 *Science* **325** 1227–30
- [19] Blakestad R, Ospelkaus C, VanDevender A, Wesenberg J, Biercuk M, Leibfried D and Wineland D 2011 *Phys. Rev. A* **84** 032314
- [20] Duan L M and Monroe C 2010 *Rev. Mod. Phys.* **82** 1209–24

- [21] Monroe C, Raussendorf R, Ruthven A, Brown K R, Maunz P, Duan L M and Kim J 2012 1–15 arXiv:1208.0391v1
- [22] Olmschenk S, Matsukevich D N, Maunz P, Hayes D and Monroe C 2009 *Science* **323** 486–9
- [23] Maunz P, Olmschenk S, Hayes D, Matsukevich D, Duan L M and Monroe C 2009 *Phys. Rev. Lett.* **102** 250502
- [24] Tanji-Suzuki H, Leroux I D, Cetina M and Simon J 2011 Interaction between atomic ensembles and optical resonators: classical description *Adv. Atom. Mol. Opt. Phys.* **60** 201–40
- [25] Thompson R J, Rempe G and Kimble H J 1992 *Phys. Rev. Lett.* **68** 1132–5
- [26] Kuhn A, Hennrich M and Rempe G 2002 *Phys. Rev. Lett.* **89** 067901
- [27] Gehr R, Volz J, Dubois G, Steinmetz T, Colombe Y, Lev B L, Long R, Estève J and Reichel J 2010 *Phys. Rev. Lett.* **104** 203602
- [28] Black A T, Thompson J K and Vuletić V 2005 *Phys. Rev. Lett.* **95** 133601
- [29] Herskind P F, Dantan A, Marler J P, Albert M and Drewsen M 2009 *Nature Phys.* **5** 494–8
- [30] Guthöhrlein G R, Keller M, Hayasaka K, Lange W and Walther H 2001 *Nature* **414** 49–51
- [31] Leibbrandt D, Labaziewicz J, Vuletić V and Chuang I 2009 *Phys. Rev. Lett.* **103** 103001
- [32] Mundt A, Kreuter A, Becher C, Leibfried D, Eschner J, Schmidt-Kaler F and Blatt R 2002 *Phys. Rev. Lett.* **89** 103001
- [33] Russo C *et al* 2009 *Appl. Phys. B* **95** 205–12
- [34] Stute A, Casabone B, Brandstätter B, Habicher D, Barros H G, Schmidt P O, Northup T E and Blatt R 2012 *Appl. Phys. B* **107** 1145–57
- [35] Keller M, Lange B, Hayasaka K, Lange W and Walther H 2004 *Nature* **431** 1075–8
- [36] Barros H G, Stute A, Northup T E, Russo C, Schmidt P O and Blatt R 2009 *New J. Phys.* **11** 103004
- [37] Stute A, Casabone B, Schindler P, Monz T, Schmidt P O, Brandstätter B, Northup T E and Blatt R 2012 *Nature* **485** 482–5
- [38] Sterk J, Luo L, Manning T, Maunz P and Monroe C 2012 *Phys. Rev. A* **85** 062308
- [39] Simon J, Tanji H, Ghosh S and Vuletić V 2007 *Nature Phys.* **3** 765–9
- [40] Tanji H, Ghosh S, Simon J, Bloom B and Vuletić V 2009 *Phys. Rev. Lett.* **103** 043601
- [41] Zhao R, Dudin Y O, Jenkins S D, Campbell C J, Matsukevich D N, Kennedy T A B and Kuzmich A 2008 *Nature Phys.* **5** 100–4
- [42] Radnaev A G, Dudin Y O, Zhao R, Jen H H, Jenkins S D, Kuzmich A and Kennedy T A B 2010 *Nature Phys.* **6** 894–9
- [43] Lamata L, Leibbrandt D, Chuang I, Cirac J, Lukin M, Vuletić V and Yelin S 2011 *Phys. Rev. Lett.* **107** 030501
- [44] Albert M, Dantan A and Drewsen M 2011 *Nature Photon.* **5** 633–6
- [45] Cirac J and Zoller P 2000 *Nature* **404** 579–81
- [46] Chiaverini J and Lybarger W 2008 *Phys. Rev. A* **77** 022324
- [47] Schmied R, Roscilde T, Murg V, Porras D and Cirac J I 2008 *New J. Phys.* **10** 045017
- [48] Brown K R, Ospelkaus C, Colombe Y, Wilson A C, Leibfried D and Wineland D J 2011 *Nature* **471** 196–9
- [49] Harlander M, Lechner R, Brownnutt M, Blatt R and Hänsel W 2011 *Nature* **471** 2–5
- [50] Schneider C, Enderlein M, Huber T and Schaetz T 2010 *Nature Photon.* **4** 772–5
- [51] Linnet R, Leroux I, Marcianti M, Dantan A and Drewsen M 2012 *Phys. Rev. Lett.* **109** 233005
- [52] Enderlein M, Huber T, Schneider C and Schaetz T 2012 *Phys. Rev. Lett.* **109** 233004
- [53] Karpa L, Bylinskii A, Gangloff D, Cetina M and Vuletić V 2013 arXiv:1304.0049
- [54] Trotzky S, Cheinet P, Fölling S, Feld M, Schnorrberger U, Rey A M, Polkovnikov A, Demler E A, Lukin M D and Bloch I 2008 *Science* **319** 295–9
- [55] Simon J, Bakr W S, Ma R, Tai M E, Preiss P M and Greiner M 2011 *Nature* **472** 307–12
- [56] García-Mata I, Zhirov O V and Shepelyansky D L 2006 *Eur. Phys. J. D* **41** 325–30
- [57] Benassi A, Vanossi A and Tosatti E 2011 *Nature Commun.* **2** 236
- [58] Pruttivarasin T, Ramm M, Talukdar I, Kreuter A and Häffner H 2011 *New J. Phys.* **13** 075012
- [59] Bermudez A, Schaetz T and Porras D 2011 *Phys. Rev. Lett.* **107** 150501
- [60] Bakr W S, Gillen J I, Peng A, Fölling S and Greiner M 2009 *Nature* **462** 74–7

- [61] Sherson J F, Weitenberg C, Endres M, Cheneau M, Bloch I and Kuhr S 2010 *Nature* **467** 68–72
- [62] Birkel G and Kassner S H W 1992 *Nature* **357** 310–3
- [63] Dubin D H E 1993 *Phys. Rev. Lett.* **71** 2753–6
- [64] Schiffer J P 1993 *Phys. Rev. Lett.* **70** 818–21
- [65] Grier A T 2011 *PhD Thesis* Massachusetts Institute of Technology
- [66] Labaziewicz J, Ge Y, Antohi P, Leibbrandt D, Brown K and Chuang I 2008 *Phys. Rev. Lett.* **100** 013001
- [67] Gangloff D, Bylinskii A, Li J, Cetina M, Karpa L and Vuletić V 2013 in preparation
- [68] Balzer C, Braun A, Hannemann T, Paape C, Ettl M, Neuhauser W and Wunderlich C 2006 *Phys. Rev. A* **73** 041407
- [69] Cetina M, Grier A, Campbell J, Chuang I and Vuletić V 2007 *Phys. Rev. A* **76** 041401
- [70] Olmschenk S, Hayes D, Matsukevich D, Maunz P, Moehring D, Younge K and Monroe C 2009 *Phys. Rev. A* **80** 022502
- [71] Cohen-Tannoudji C, Dupont-Roc J and Grynberg G 1992 *Atom–Photon Interactions: Basic Processes and Applications* (New York: Wiley)
- [72] Schnorrberger U, Thompson J D, Trotzky S, Pugatch R, Davidson N, Kuhr S and Bloch I 2009 *Phys. Rev. Lett.* **103** 033003
- [73] Berkeland D J, Miller J D, Bergquist J C, Itano W M and Wineland D J 1998 *J. Appl. Phys.* **83** 5025